Theory of microwave spectroscopy of Andreev bound states with a Josephson junction

L. Bretheau,[1,*] Ç. Ö. Girit,[1] M. Houzet,[2,3] H. Pothier,[1,†] D. Esteve,[1] and C. Urbina[1]

[1]*Quantronics Group, Service de Physique de l'État Condensé (CNRS, URA 2464), IRAMIS, CEA-Saclay, 91191 Gif-sur-Yvette, France*

[2]*Université Grenoble Alpes, INAC-SPSMS, F-38000 Grenoble, France*

[3]*CEA, INAC-SPSMS, F-38000 Grenoble, France*

(Received 24 June 2014; revised manuscript received 22 September 2014; published 8 October 2014)

We present a microscopic theory for the current through a tunnel Josephson junction coupled to a nonlinear environment, which consists of an Andreev two-level system coupled to a harmonic oscillator. It models a recent experiment [Bretheau, Girit, Pothier, Esteve, and Urbina, Nature (London) **499**, 312 (2013)] on photon spectroscopy of Andreev bound states in a superconducting atomic-size contact. We find the eigenenergies and eigenstates of the environment and derive the current through the junction due to inelastic Cooper pair tunneling. The current-voltage characteristic reveals the transitions between the Andreev bound states, the excitation of the harmonic mode that hybridizes with the Andreev bound states, as well as multiphoton processes. The calculated spectra are in fair agreement with the experimental data.

DOI: 10.1103/PhysRevB.90.134506 PACS number(s): 74.45.+c, 73.23.−b, 74.50.+r

I. INTRODUCTION

The Josephson effect, predicted and observed 50 years ago in superconducting tunnel junctions [1–3], describes the nondissipative supercurrent that results from the coherent coupling between superconductors separated by a thin insulating barrier. Since then the supercurrent has been observed in many other weak links such as point contacts, semiconducting nanowires, carbon nanotubes, graphene sheets, and thin ferromagnetic layers [4]. Microscopically the Josephson coupling is established through fermionic states whose energies depend on the superconducting phase difference δ across the weak link. For a weak link shorter than the superconducting coherence length ξ, these so-called Andreev bound states (ABS) have energies smaller than the superconducting gap Δ and are therefore localized at the weak link over a distance of the order of ξ [5–8]. In a single-channel weak link, there is only one pair of ABS, $|-\rangle$ and $|+\rangle$, with energies $\mp E_A$ [see Fig. 1(a)], where

$$E_A = \Delta\sqrt{1-\tau\sin^2(\delta/2)}. \tag{1}$$

Here δ is the superconducting phase difference and τ is the transmission probability for electrons in the normal state. The phase dependence gives rise to opposite supercurrents $\mp(1/\varphi_0)(\partial E_A/\partial\delta)$ in the ground and excited states (with $\varphi_0 = \hbar/2e$ the reduced flux quantum). This pair of states can be seen as a spin-1/2 and introduces an internal degree of freedom to Josephson weak links.

At zero temperature only the lower energy state $|-\rangle$ is occupied. This ground state has been probed through measurements of the current-phase relation in superconducting atomic contacts [9]. The direct observation of the higher energy state $|+\rangle$ has been achieved only recently [10,11]. In the experiment of Ref. [10], a voltage-biased Josephson junction was used as an on-chip spectrometer (see Fig. 2). The dissipative subgap current through the Josephson junction is due to inelastic tunneling of Cooper pairs, the released energy being absorbed in the environment (see Fig. 1). Current peaks are then observed at energies corresponding to the eigenenergies of the environment.

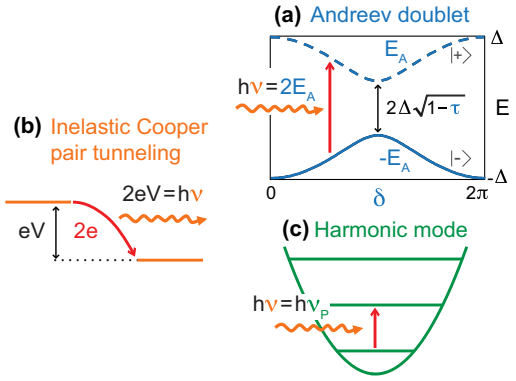

FIG. 1. (Color online) Principle of the photon spectroscopy of Andreev bound states. (a) Phase (δ) dependence of the Andreev levels with energies $\mp E_A$ in a short conduction channel of transmission τ. Δ is the superconducting gap. (b) A Cooper pair tunneling across the spectrometer junction releases energy $2eV$ as a photon of frequency ν, which is absorbed either in the atomic contact by exciting the Andreev transition at energy $2E_A$ (a) or in a harmonic oscillator mode (c) present in the embedding circuit of the atomic contact (see Fig. 2).

In practice, the environment was an asymmetric SQUID formed by a superconducting atomic contact in parallel with a second Josephson junction (see Fig. 2). This environment can be modeled as a spin-1/2 degree of freedom (the Andreev doublet) coupled with a harmonic mode (the plasma mode of the Josephson junction) (see Fig. 1). The goal of the present work is to reach a quantitative understanding of the measured spectra.

The rest of the paper is organized as follows. Section II gives a Hamiltonian description of the circuit schematized in Fig. 2. The spectrometer Hamiltonian is then treated as a perturbation, and following previous work [12–17], the atomic contact is treated under the assumption of small phase fluctuations. In Sec. III, the resulting spin-boson Hamiltonian

*Present address: Laboratoire Pierre Aigrain, Ecole Normale Supérieure, CNRS (UMR 8551), 75231 Paris Cedex 05, France.

†hugues.pothier@cea.fr

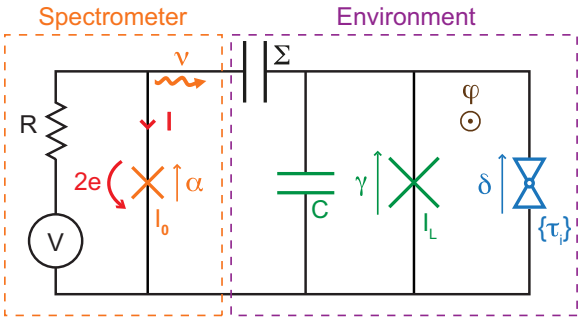

FIG. 2. (Color online) Simplified diagram of the experimental setup. A voltage-biased Josephson junction (orange cross) is used as a spectrometer. It emits microwaves in its environment, an atomic SQUID formed by an ancillary Josephson junction (green cross in parallel with a capacitor C) and an atomic point contact (blue triangles) of channel transmission probabilities $\{\tau_i\}$. The absorption of a photon by the environment is accompanied by the transfer of a Cooper pair through the spectrometer. The phases γ and δ across the SQUID junction and the atomic contact are linked by the external reduced flux φ threading the loop: $\delta = \gamma + \varphi$. The phase across the spectrometer is given by $\alpha = \gamma + 2eVt$.

of the environment is solved numerically, and the calculated current spectra are compared with the experimental ones. Finally, in Sec. IV the Hamiltonian is solved analytically in the Jaynes-Cummings approximation. Some perspectives are discussed in the conclusion.

II. MODEL

A. Setup

The setup used in the experiment [10] is shown schematically in Fig. 2. On the left-hand side, a voltage-biased Josephson junction (critical current $I_0 = 48$ nA) is used as a spectrometer. It is biased with a voltage source V in series with a resistor $R = 2\,\mathrm{k}\Omega$. It radiates microwaves at the Josephson frequency $\nu = 2eV/h$ [18], which can be absorbed by its electromagnetic environment, an atomic-SQUID formed by an atomic point contact in parallel with a second Josephson junction. The critical current $I_L = 1.06$ μA of this second junction is much larger than those of the spectrometer junction and of a one-atom contact. An external superconducting coil is used to apply a dc flux $\phi = \varphi_0\varphi$ through the SQUID loop. The capacitance $C = 280$ fF corresponds to the sum of the junctions capacitors. The atomic-SQUID and the spectrometer are coupled through a capacitor $\Sigma \sim 30$ pF. Whereas it behaves as an open circuit from the dc point of view and ensures that the dc voltage V falls on the spectrometer, it can be considered as a short for the Josephson radiation in the explored frequency range $[\nu \gg \nu_p(C/\Sigma)^{1/2} \sim 2$ GHz, with ν_p the plasma frequency of the SQUID junction].

B. Hamiltonian of the circuit

Neglecting the coupling capacitor and the bias resistor, the circuit represented in Fig. 2 can be described with the Hamiltonian $H = H_{\mathrm{spec}} + H_{\mathrm{SQ}}$. The first term $H_{\mathrm{spec}} = -E_J\cos(\gamma + 2eVt)$ corresponds to the spectrometer with Josephson energy $E_J = \varphi_0 I_0$. The voltage drop across the spectrometer junction induces a superconducting phase difference $\alpha = \gamma + 2eVt$, with γ the phase at the SQUID junction [19]. The coupling with the SQUID occurs through the phase operator γ.

The Hamiltonian

$$H_{\mathrm{SQ}} = E_C N^2 - E_L\cos(\gamma) + H_A(\delta) \tag{2}$$

accounts for the SQUID. The operator N is the number of Cooper pairs that have crossed the tunnel junction; N and γ are conjugated operators: $[\gamma, N] = i$. $E_C = 2e^2/C$ is the charging energy for pairs and E_L is the Josephson energy of the SQUID junction. The last term in Eq. (2) describes the atomic contact. The phase $\delta = \varphi + \gamma$ across the atomic contact differs from γ by φ, the reduced flux. For a single channel contact, and neglecting excitations which involve quasiparticles in the continuum, the Andreev Hamiltonian is [13,14]

$$\begin{aligned} &H_A = -\Delta(\mathrm{Im}U\,\sigma_y + \mathrm{Re}U\,\sigma_z), \\ &\text{with}\quad U = \left[\cos\left(\frac{\delta}{2}\right) + i\sqrt{1-\tau}\,\sin\left(\frac{\delta}{2}\right)\right] e^{-i\sqrt{1-\tau}\frac{\delta}{2}}, \end{aligned} \tag{3}$$

where the Pauli matrices $\sigma_{x,y,z}$ act in a 2×2 subspace corresponding to the two ABS. The physics of the ABS is therefore analogous to that of a spin-1/2 in a magnetic field whose magnitude $\Delta|U| = E_A$ and direction depend on the superconducting phase difference δ across the contact. The eigenstates of H_A are the ABS $|\pm\rangle$, with eigenenergies $\pm E_A$ [see Eq. (1) and Fig. 1(a)].

C. Andreev spin and plasma boson

In the experiment [10], due to the large asymmetry $E_L \gg E_A$, the phase dynamics is essentially ruled by the SQUID junction. The size of the phase fluctuations is determined by the dimensionless parameter $z = (E_C/2E_L)^{1/2} \ll 1$. Therefore, following Ref. [12], we may treat the SQUID junction as a linear inductor and retain only the lowest order coupling ($\propto\sqrt{z}$) between the SQUID junction and the atomic contact in Eq. (2). Namely,

$$H_{\mathrm{SQ}} \approx E_C N^2 + E_L\gamma^2/2 + H_A(\varphi) + \varphi_0\gamma C_A(\varphi), \tag{4}$$

where $C_A = \varphi_0^{-1}\partial H_A/\partial\delta$ is the Andreev current operator. Hence, the parallel combination of the SQUID junction and the capacitor C forms a harmonic oscillator of resonant frequency $\nu_p = \sqrt{2E_L E_C}/h$ [see Fig. 1(c)]. Switching to second quantization, its Hamiltonian reads $h\nu_p(a^\dagger a + \frac{1}{2})$, where the phase $\gamma = \sqrt{z}\left(a + a^\dagger\right)$ is linked to the annihilation and creation operators a and $a^\dagger$ of the plasma mode of the SQUID.

In the basis of the Andreev states $\{|-\rangle, |+\rangle\}$, the SQUID Hamiltonian finally reads

$$H_{\mathrm{SQ}} = h\nu_p\left(a^\dagger a + \tfrac{1}{2}\right) - E_A\sigma_z + (a + a^\dagger)(\Omega_x\sigma_x + \Omega_z\sigma_z), \tag{5}$$

where

$$\Omega_z = \Delta\sqrt{z}\frac{\tau\sin(\varphi)}{4\sqrt{1-\tau\sin^2\left(\frac{\varphi}{2}\right)}} \tag{6}$$

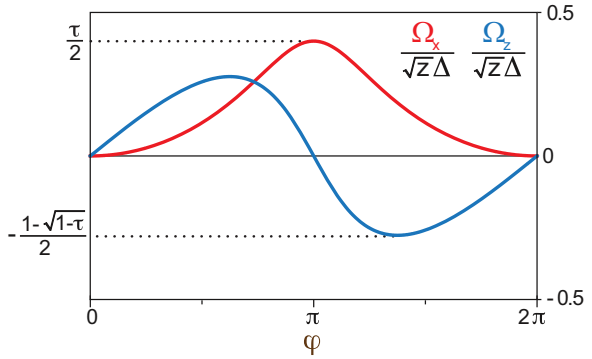

FIG. 3. (Color online) Phase dependence of the coupling energies Ω_x (red) and Ω_z (blue) in units of $\sqrt{z}\Delta$, for $\tau = 0.8$.

and $\Omega_x = \Omega_z\sqrt{1-\tau}\tan\left(\frac{\varphi}{2}\right)$. The phase dependence of these coupling energies is represented in Fig. 3.

The spin-boson Hamiltonian (5) yields a discrete eigenspectrum which results from the hybridization of the bosonic plasma mode in the SQUID junction and the Andreev spin-1/2 degree of freedom in the atomic contact [see Fig. 4(a)]. The term $\propto\Omega_x$ allows transitions between Andreev states. It is minimum at $\varphi = 0$ and maximum at $\varphi = \pi$. Note that the flux modulation of the SQUID plasma frequency due to the contribution of the effective inductance of the atomic contact would appear as a higher order effect in z.

D. Incoherent Cooper pair current

The global circuit Hamiltonian H cannot be diagonalized analytically. Along the lines of $P(E)$ theory for dynamical Coulomb blockade [20,21], the spectrometer may be treated as a perturbation. The dc current I flowing through the spectrometer is calculated using the current operator $I_0\sin(\gamma + 2eVt)$ and perturbation theory up to the second order in E_J. At zero temperature and for $V > 0$,

$$\frac{I(V)}{I_0} = \frac{\pi}{2}E_J\sum_k |\langle k|e^{i\gamma}|0\rangle|^2\delta\left[(E_k - E_0) - 2eV\right], \qquad (7)$$

where $|k\rangle$ are the eigenstates of $H_{\rm SQ}$ with energy E_k. Equation (7) accounts for incoherent Cooper pair tunneling through the junction's barrier at rate $I/2e$, provided that the energy $2eV$ matches an excitation energy of the junction environment [see Fig. 1(b)]. As in $P(E)$ theory for zero temperature, we assume that, before each tunneling event, the environment has relaxed to its ground state $|0\rangle$.

In $P(E)$ theory [20,21], the environment is purely electromagnetic, linear and is described by an impedance $Z(\omega)$. Equation (7) then simplifies and gives the current as a function of $\mathrm{Re}Z(\omega)$. In particular, this would yield current peaks at $2eV = nh\nu_p$ (n integer), with a width related to the quality factor of the bosonic plasma mode of frequency ν_p.

Such an approach is not possible here due to the strong nonlinearity of the Andreev degree of freedom. As the model does not include dissipation, the spin-boson Hamiltonian $H_{\rm SQ}$ yields a discrete spectrum. Then, Eq. (7) predicts infinitely sharp dc current peaks at the excitation energies of $H_{\rm SQ}$. A finite broadening of each of the peaks may be introduced phenomenologically with the substitution $\delta(E - E_0) \to (\Gamma/\pi)/[(E - E_0)^2 + \Gamma^2]$ in Eq. (7). While the model is unable to predict the amplitude of the linewidth Γ, it should be large enough for the incoherent Cooper pair current through the spectrometer junction to be small, $I \ll I_0$, so that perturbation theory is valid. Near voltage $V = \epsilon_k/(2e)$, where $\epsilon_k = E_k - E_0$, this condition reads $(E_J/\Gamma)P_k \ll 1$, with transition probability $P_k = |\langle k|e^{i\gamma}|0\rangle|^2$.

III. SPECTRA CALCULATION

A. Numerical resolution

The spectrum of Hamiltonian (5) can be obtained numerically. To do so, we write it as a matrix in the basis $\{|\sigma,n\rangle\}$, where $\sigma = \pm$ accounts for the Andreev spin-1/2 and n is the plasmon occupation number, and truncate to the lower energy states. By numerical resolution of a 14×14 Hamiltonian matrix ($n \leqslant 6$), we have computed all the resonances of energy smaller than 2Δ and the corresponding transition probabilities P_k. Figure 4 shows the excitation spectrum (b) and the transition probabilities (c) for the transitions indicated in (a), for a channel of transmission $\tau = 0.98$. In the experiment, the superconducting gap energy is $\Delta/h \simeq 43$ GHz, the charging energy is $E_C/h \simeq 270$ MHz and the Josephson energy of the SQUID junction is $E_L/h \simeq 900$ GHz, leading to $z \simeq 0.012$. Note that E_L is renormalized as $E_L = \varphi_0(I_L + 2\varphi_0/L)$, where $L/2 = 0.44$ nH is a parallel inductor (not shown in Fig. 2) accounting for a 1.35-mm-long aluminum connecting wire present in the actual geometry of the sample.

B. Incorporating line broadening

The experimental data displayed in the right panels of Fig. 5 show broad lines. One notices that the transition solely concerning the plasma mode is already broad, which indicates that this mode is subject to dissipation and/or dephasing; note also that voltage fluctuations across the spectrometer junction can limit the energy resolution [22]. To account for the broadening of the energy levels of $H_{\rm SQ}$ one should at least include the coupling of the plasma mode to a dissipative bath. Treating the latter as an infinite collection of harmonic oscillators, as it is usually done, would lead to a complex spin-boson problem without analytical solution. Here we simply introduce in Eq. (7) a phenomenological Lorentzian broadening, cf. Sec. II D. By fitting the plasma resonance peak, we found $\Gamma/h = 2$ GHz, which we used for all the calculated lines shown in the left panels of Fig. 5.

C. Comparison with experiment

In experiments atomic contacts have several channels. We extend the model to contacts with multiple channels by adding an Andreev term (3) for each channel to the Hamiltonian. This Hamiltonian describes the physics of $\mathcal{N}$ spins coupled to the same bosonic mode but not directly coupled to each other. All the approximations made before are still valid [23]. Figure 5 compares the calculated spectra (left) with the experimental ones from Ref. [10] (right), for two different atomic contacts $AC1$ (transmissions 0.942, 0.26) and $AC2$

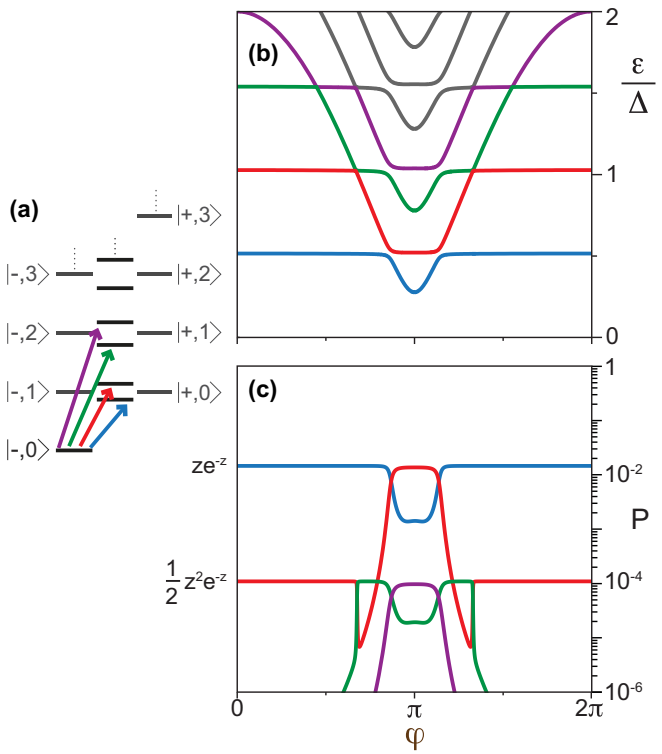

FIG. 4. (Color online) (a) Energy spectrum diagrams of $H_{\rm SQ}$ for a single channel: each state is labeled $|-,n\rangle$ or $|+,n\rangle$ for the Andreev pair in the ground $(-)$ or excited $(+)$ state and n photons in the plasma mode. At degeneracy $2E_A = h\nu_p$, the plasma and Andreev modes hybridize, which leads to an avoided crossing visible in (b). (b) and (c) Excitation energies ϵ (in units of Δ) (b) and transition probabilities P (c) of the first resonances, as a function of the reduced flux φ, for a channel of transmission $\tau = 0.98$. These lines are obtained by numerical resolution of a 14×14 Hamiltonian matrix. Each color encodes a transition from the ground state towards a different excited state, as represented in (a).

(transmissions 0.985, 0.37). The theory is obtained with the numerical method sketched before, still using seven photon levels (28×28 matrix).

The model describes both the Andreev transitions $|-,0\rangle \rightarrow |+,0\rangle$, of energy $2E_A$ (V-shaped lines), and the plasma transition $|-,0\rangle \rightarrow |-,1\rangle$, of energy $h\nu_p$ (red horizontal line at $0.51\,\Delta$). It also describes the higher harmonic transitions: $|-,0\rangle \rightarrow |+,1\rangle$, of energy $2E_A + h\nu_p$ (replica of the Andreev transition, shifted up by $0.51\,\Delta$) and $|-,0\rangle \rightarrow |-,2\rangle$, of energy $2h\nu_p$ (white horizontal line at $1.02\,\Delta$). These processes correspond to the tunneling of one Cooper pair and emission of two photons. They are less probable and result in fainter transitions as seen both in experiment and calculation. Theory also accounts for the anticrossings arising from the coupling between the Andreev spin and the plasma boson. Only crossings of transition lines involving the same number of photons show significant hybridization, in good agreement with the data.

Extra phase-independent current at $2eV \lesssim \Delta/2$ in the experimental data is attributed to the coupling to uncontrolled environmental modes outside of the SQUID.

Finally, the global weakening of the signal at high V is well captured by the model. This weakening is due to the lower impedance of the SQUID capacitance compared to its inductance at frequencies larger than the plasma frequency. However, the agreement for the amplitude and width of the different peaks is not quantitative. Having set the width to 2 GHz, a correct peak amplitude is only obtained when multiplying theory by a factor 0.6. A rigorous treatment of dissipation is needed. This could be achieved by adding an electromagnetic impedance with a dissipative component in parallel with the SQUID.

IV. ANDREEV-PLASMA MODE HYBRIDIZATION

We use the rotating wave approximation, valid in the vicinity of the degeneracy $h\nu_p = 2E_A$, to obtain analytical expressions for the excitation energies and transition rates. The Hamiltonian can be approximated by the Jaynes-Cummings model [24,25]:

$$H_{\rm SQ}^{\rm JC} = h\nu_p \left(a^\dagger a + \tfrac{1}{2}\right) - E_A\sigma_z + \Omega_x(a\sigma_+ + a^\dagger\sigma_-), \qquad (8)$$

where $\sigma_\pm = \frac{1}{2}(\sigma_x \mp i\sigma_y)$. Then, by block diagonalization in the subspace $\{|+,n\rangle, |-,n+1\rangle\}$, one derives the eigenstates and eigenenergies and computes the excitations energies and transition probabilities.

To fourth order in $\sqrt{z}$, the current (7) through the spectrometer displays four peaks

$$\frac{I(V)}{I_0} = \frac{\pi}{2}E_J \sum_{\sigma=\pm;n=1,2} P_n^\sigma \delta\left(2eV - \epsilon_n^\sigma\right) \qquad (9)$$

at the bias voltages matching the excitation energies (see top panel of Fig. 6):

$$\epsilon_n^\pm = E_A + \left(n - \tfrac{1}{2}\right)h\nu_p \pm W_n, \qquad (10)$$

with $W_n = \sqrt{(E_A - \frac{1}{2}h\nu_p)^2 + n\Omega_x^2}$. The amplitudes of the current peaks are proportional to the transition probabilities (see bottom panel of Fig. 6):

$$\begin{aligned} P_n^- &= \frac{1}{n!}z^n e^{-z}\cos^2\left(\frac{\theta_n}{2}\right), \\ P_n^+ &= \frac{1}{n!}z^n e^{-z}\sin^2\left(\frac{\theta_n}{2}\right), \end{aligned} \qquad (11)$$

with $\theta_n = \arctan\left(n\Omega_x / W_0\right)$.

These peaks correspond to excitations towards composite states, resulting from the hybridization of the plasma and Andreev modes [see Fig. 4(a)]. The first two resonances in Eq. (9) correspond to the excitation with a single photon of the hybridized Andreev ($2E_A$) and plasma mode ($h\nu_p$); the last two resonances correspond to the excitation of higher harmonic modes at $2h\nu_p$ and $h\nu_p + 2E_A$. These two-photon processes are possible because the spectrometer, a Josephson tunnel junction, is a nonlinear emitter. They correspond to the tunneling of one Cooper pair and emission of two photons. Note that far from degeneracy, using perturbation theory with $z \ll 1$, one finds for the plasma resonance and its harmonic the transition probabilities ze^{-z} and $\frac{1}{2}z^2e^{-z}$. These amplitude

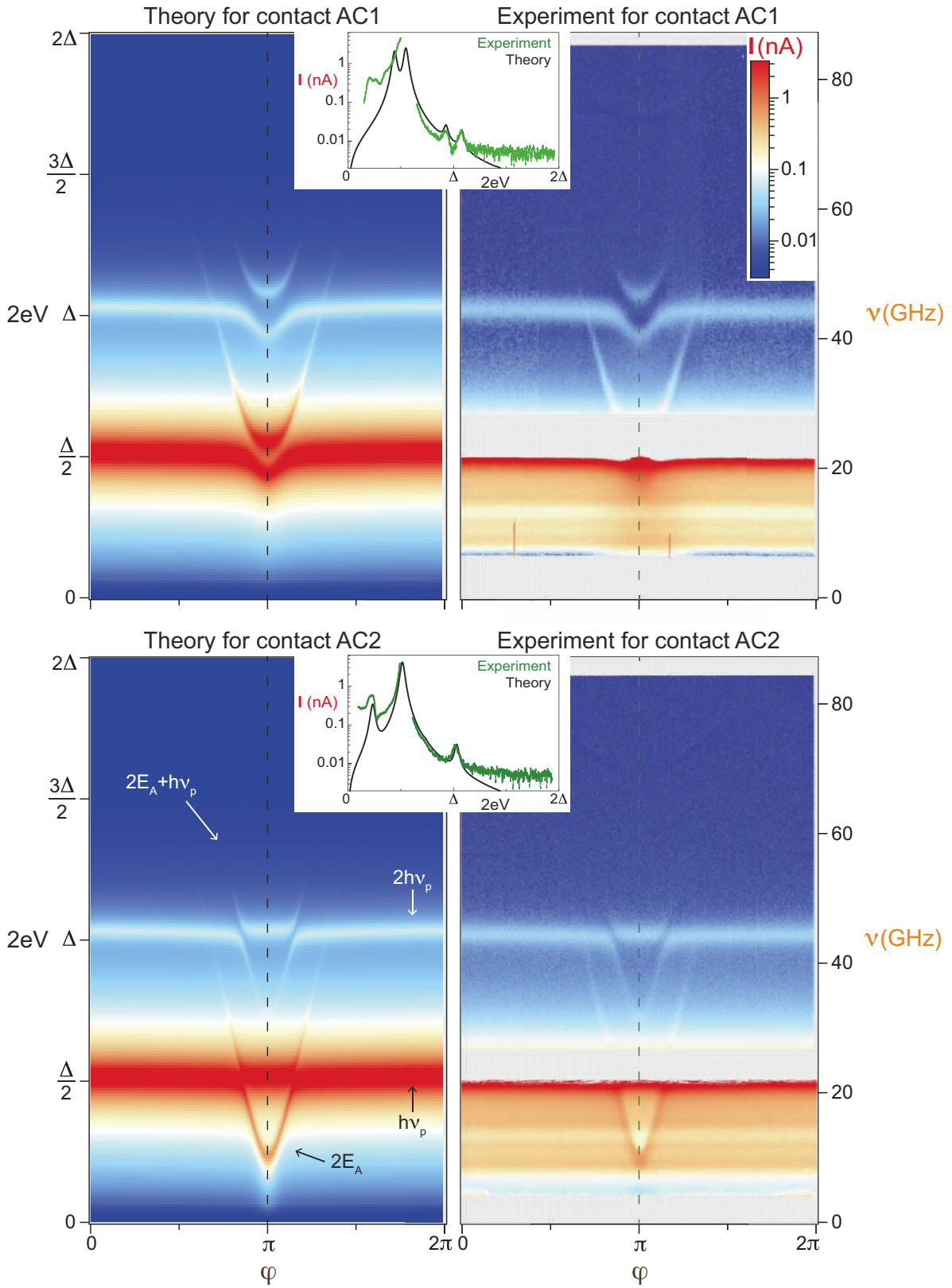

FIG. 5. (Color online) Comparison between calculated (left) and experimental (right) spectra $I(\varphi, V)$ for contact $AC1$ (transmissions 0.942, 0.26) (top) and $AC2$ (transmissions 0.985, 0.37) (bottom). The two insets show theoretical (black lines) and experimental (green lines) $I(V)$ cuts for $\varphi = \pi$, for each contact. Right: The experimental spectra are extracted from Fig. 3 in Ref. [10]. The gray regions at $\nu < 4$ GHz and around 25 GHz are not accessible because there the biasing of the spectrometer is unstable. Left: The calculated spectra are obtained using Eq. (7) with a phenomenological damping parameter $\Gamma/h = 2$ GHz. The calculated currents have been multiplied by 0.6 to match the measured ones. The transition probabilities and excitation energies are computed numerically, using seven photon levels in the plasma mode.

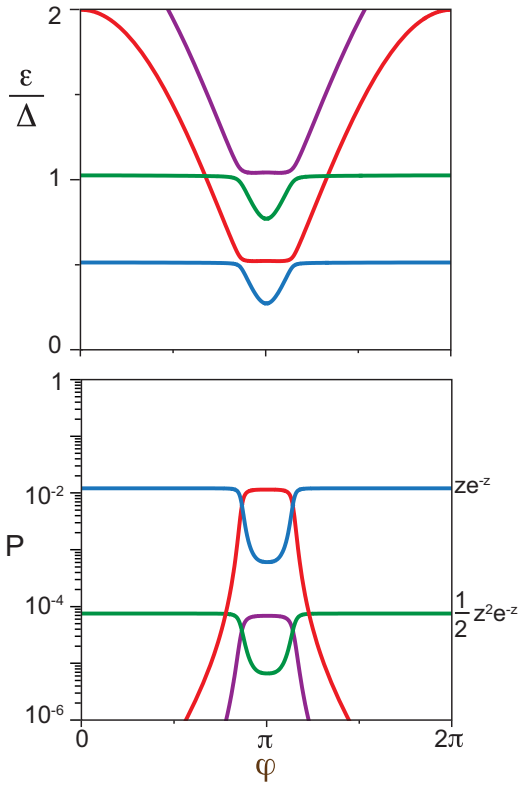

FIG. 6. (Color online) Excitation energies ϵ (in units of Δ) (top) and transition probabilities P (bottom) of the first resonances, as a function of the reduced flux φ, in the Jaynes-Cummings approximation for a channel of transmission $\tau = 0.98$. Each color encodes a transition towards a different state, as shown in Fig. 4(a).

are consistent with the Poisson distribution found at arbitrary z in the $P(E)$ derivation with a bosonic mode [21].

It is worth mentioning that the Jaynes-Cummings model gives an excellent description, even far from degeneracy when $|W_0| \gg h\nu_p$. There, the error made in energy scales as $\Omega_x/\left(2E_A + h\nu_p\right)$, and is in general negligible. However, this model fails to predict the anticrossing between the second harmonic of the plasma resonance and the Andreev resonance at $2h\nu_p = 2E_A$ (red and green lines in Fig. 6). In practice this correction is one order of magnitude smaller than the anticrossing at $h\nu_p = 2E_A$ and is not seen in the experiment [10]. Note however that the derivation in the case of multiple channels is much more involved when more than one Andreev transition crosses the plasma resonance.

V. CONCLUSIONS AND PERSPECTIVES

In conclusion, we have treated inelastic Copper pair tunneling through the emitter junction using perturbation theory in its coupling with the environment, and calculated the environmental transition energies and probabilities by diagonalization of the SQUID Hamiltonian. This Hamiltonian contains a spinlike term describing the atomic contact and which is coupled to a harmonic term for the plasma mode of the SQUID junction. The calculated spectra are in fair agreement with the experimental ones. However, this theory could benefit from several extensions.

First of all, the atomic contact Hamiltonian was restricted to a two-level system Hamiltonian, by neglecting excitations which involve quasiparticles in the continuum. In particular, quasiparticle trapping, which was measured in a similar experiment [11], leaves the Andreev doublet in a long-lived "odd" state for which both the Andreev states are either occupied or empty [26], with time scales in the millisecond range [27]. It limits the Andreev transition rate and therefore reduces the corresponding dc current. On the other hand, transitions from the Andreev bound states to the continuum were measured on the same contacts using another detection method [11]. They do not contribute to the dc current and were not seen in the experiment described in Ref. [10] due to the long lifetime of the odd states. To deal with all the Andreev excitations on the same footing, one must consider the full Hamiltonian of the atomic contact, as done in recent works [17,28].

Second, the description used here for the environment eigenstates and for the spectrometer is far from being complete. As discussed above, this is a difficult problem for two reasons: (i) the coupling of a two-level system to a dissipative resonator is not known analytically, and (ii) the $I(V)$ characteristic of a Josephson junction coupled to a resonator is not generically known when the perturbative expansion in E_J is not valid, despite recent progress along this direction [29]. Although the second order expansion is valid for the data discussed here since the Cooper pair current is small ($I \ll I_0$), higher order contributions corresponding to the transfer of more than one Cooper pair emitting several photons were observed in other experiments [11,30].

Finally, it was also assumed in the model that the environment is in its ground state each time a Cooper pair tunnels. This requires the relaxation time of the excited environment states to be shorter than the inverse tunnel rates. When this is not the case, the environment modifies the tunneling process. For the harmonic oscillator bosonic mode, this could lead to stimulated emission and lasing. For the Andreev two-level system, this could saturate absorption and reduce the Cooper pair current through the spectrometer junction. A regime in which the Andreev two-level system would coherently exchange an excitation with the Josephson junction can also be envisioned.

ACKNOWLEDGMENTS

We thank Sebastian Bergeret, Juan Carlos Cuevas, Andrew C. Doherty, Alfredo Levy Yeyati, Fabien Portier, Yuli Nazarov, and Vitaly Shumeiko for enlightening discussions. We gratefully acknowledge help from other members of the Quantronics group. This work was partially financed by ANR through projects DOC-FLUC (ANR-09-BLAN-0199-01), MASH (ANR-12-BS04-0016), and ANR-11-JS04-003-01 GLASNOST. The research leading to these results has received funding from the People Programme (Marie Curie Actions) of the European Union's Seventh Framework Programme (FP7/2007-2013) under REA grant agreement No. PIIF-GA-2011-298415.

[1] J. Nicol, S. Shapiro, and P. H. Smith, Phys. Rev. Lett. **5**, 461 (1960).
[2] B. D. Josephson, Phys. Lett. **1**, 251 (1962).
[3] P. W. Anderson and J. M. Rowell, Phys. Rev. Lett. **10**, 230 (1963).
[4] A. A. Golubov, M. Y. Kupriyanov, and E. Il'ichev, Rev. Mod. Phys. **76**, 411 (2004).
[5] I. O. Kulik, Sov. Phys. JETP **30**, 944 (1970).
[6] A. Furusaki and M. Tsukada, Solid State Commun. **78**, 299 (1991).
[7] P. F. Bagwell, Phys. Rev. B **46**, 12573 (1992).
[8] C. W. J. Beenakker, Phys. Rev. B **46**, 12841 (1992).
[9] M. L. Della Rocca, M. Chauvin, B. Huard, H. Pothier, D. Esteve, and C. Urbina, Phys. Rev. Lett. **99**, 127005 (2007).
[10] L. Bretheau, Ç. Ö. Girit, H. Pothier, D. Esteve, and C. Urbina, Nature (London) **499**, 312 (2013).
[11] L. Bretheau, Ç. Ö. Girit, C. Urbina, D. Esteve, and H. Pothier, Phys. Rev. X **3**, 041034 (2013).
[12] M. A. Desposito and A. Levy Yeyati, Phys. Rev. B **64**, 140511 (2001).
[13] A. Zazunov, V. S. Shumeiko, E. N. Bratus, J. Lantz, and G. Wendin, Phys. Rev. Lett. **90**, 087003 (2003).
[14] A. Zazunov, V. S. Shumeiko, G. Wendin, and E. N. Bratus, Phys. Rev. B **71**, 214505 (2005).
[15] F. S. Bergeret, P. Virtanen, T. T. Heikkilä, and J. C. Cuevas, Phys. Rev. Lett. **105**, 117001 (2010).
[16] G. Romero, I. Lizuain, V. S. Shumeiko, E. Solano, and F. S. Bergeret, Phys. Rev. B **85**, 180506 (2012).
[17] F. Kos, S. E. Nigg, and L. I. Glazman, Phys. Rev. B **87**, 174521 (2013).
[18] The voltage drop across the bias resistor is here neglected, which is valid in the limit $R_b I \ll V$.
[19] At low enough frequency for the impedance of the coupling capacitor to be the dominant one, the dc voltage drop across the bias resistor and across the SQUID can be neglected.
[20] M. H. Devoret, D. Esteve, H. Grabert, G.-L. Ingold, H. Pothier, and C. Urbina, Phys. Rev. Lett. **64**, 1824 (1990).
[21] G.-L. Ingold and Y. V. Nazarov, in *Single Charge Tunneling*, edited by H. Grabert and M. H. Devoret (Plenum, New York, 1992), Vol. 294, pp. 21–107.
[22] K. K. Likharev *Dynamics of Josephson Junctions and Circuits* (Gordon and Breach, New York, 1986).
[23] This is true as long as the whole atomic contact critical current remains small as compared to the critical current of the SQUID junction. Typically, a three-channel contact has a critical current below 100 nA, which is 10 times smaller than the critical current of the SQUID junction.
[24] E. T. Jaynes and F. W. Cummings, Proc. IEEE **51**, 89 (1963).
[25] B. W. Shore and P. L. Knight, J. Mod. Opt. **40**, 1195 (1993).
[26] N. M. Chtchelkatchev and Y. V. Nazarov, Phys. Rev. Lett. **90**, 226806 (2003).
[27] M. Zgirski, L. Bretheau, Q. Le Masne, H. Pothier, D. Esteve, and C. Urbina, Phys. Rev. Lett. **106**, 257003 (2011).
[28] D. G. Olivares *et al.*, Phys. Rev. B **89**, 104504 (2014).
[29] V. Gramich, B. Kubala, S. Rohrer, and J. Ankerhold, Phys. Rev. Lett. **111**, 247002 (2013).
[30] L. Bretheau, Ph.D. thesis, Ecole Polytechnique, 2013, available online at http://hal.archives-ouvertes.fr/tel-00772851/.